

SafeDrive: Fine-Grained Safety Reasoning for End-to-End Driving in a Sparse World

Junho Kim Jiyong Oh Seunghoon Yu Hongjae Shin Donghyuk Kwak Jun Won Choi[†]
Seoul National University, Republic of Korea

{jhhkim, jyoh, shyu, hjshin, dhkwak}@adr.snu.ac.kr junwchoi@snu.ac.kr

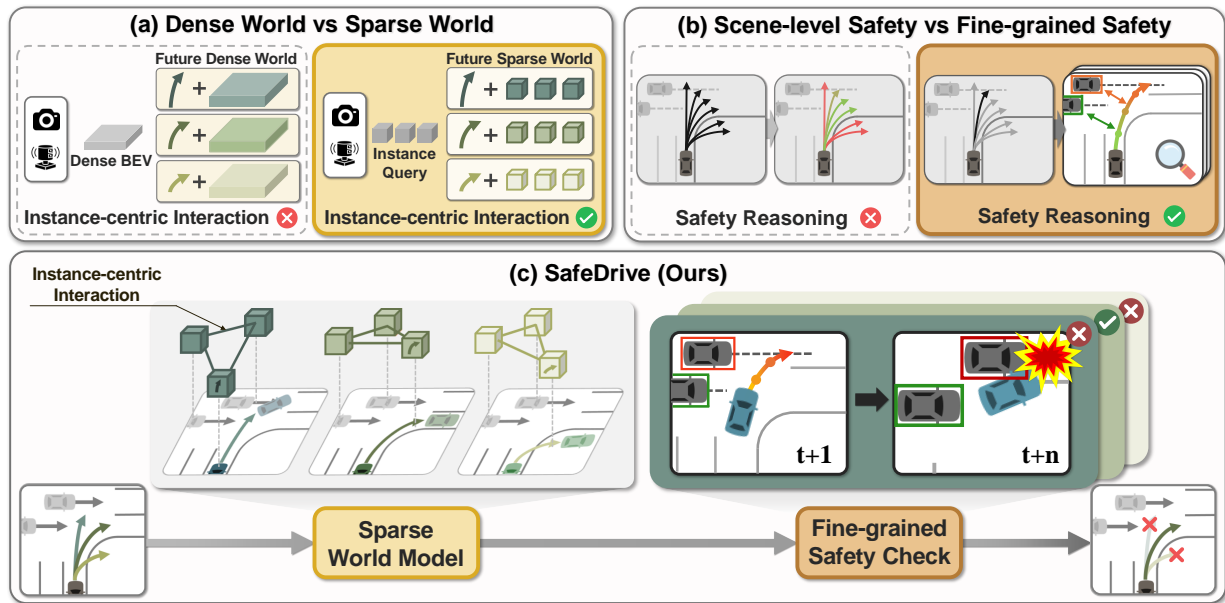


Figure 1. **Comparison of end-to-end planning paradigms and the SafeDrive framework.** (a) Dense world models provide limited modeling of instance-centric interactions, whereas sparse world models capture them effectively. (b) Scene-level safety evaluation is coarse, while fine-grained evaluation identifies the specific agents and timestamps associated with potential risks. (c) SafeDrive leverages a sparse world model and fine-grained safety reasoning to generate safe trajectories.

Abstract

The end-to-end (E2E) paradigm, which maps sensor inputs directly to driving decisions, has recently attracted significant attention due to its unified modeling capability and scalability. However, ensuring safety in this unified framework remains one of the most critical challenges. In this work, we propose SafeDrive, an E2E planning framework designed to perform explicit and interpretable safety reasoning through a trajectory-conditioned Sparse World Model. SafeDrive comprises two complementary networks: the Sparse World Network (SWNet) and the Fine-grained

Reasoning Network (FRNet). SWNet constructs trajectory-conditioned sparse worlds that simulate the future behaviors of critical dynamic agents and road entities, providing interaction-centric representations for downstream reasoning. FRNet then evaluates agent-specific collision risks and temporal adherence to drivable regions, enabling precise identification of safety-critical events across future timesteps. SafeDrive achieves state-of-the-art performance on both open-loop and closed-loop benchmarks. On NAVSIM, it records a PDMS of 91.6 and an EPDMS of 87.5, with only 61 collisions out of 12,146 scenarios (0.5%). On Bench2Drive, SafeDrive attains a 66.8% driving score.

[†]Corresponding author

1. Introduction

Autonomous driving ultimately places safety at its core, as even rare failures can lead to critical risks in real-world environments. Traditional modular pipelines, which execute perception, prediction, and planning in sequence, often suffer from error propagation between modules and may result in unsafe or inconsistent driving behaviors. To alleviate these issues, end-to-end (E2E) autonomous driving has emerged as a unified learning framework that directly maps sensor inputs to driving decisions. By integrating all components into a single model, E2E models reduce cross-module dependencies and improve robustness against accumulated errors, leading to more stable and reliable driving outcomes. This integration and scalability have further accelerated the adoption of imitation learning [3, 9, 12, 13, 33, 34, 38, 46], enabling models to learn expert driving behaviors from large-scale data. Nevertheless, imitation learning still faces fundamental limitations, as it primarily focuses on reproducing expert behaviors without explicitly reasoning about the underlying factors that lead to unsafe behaviors or potential risks.

To incorporate safety into end-to-end decision making, recent studies [1, 17, 23, 25, 44] have proposed trajectory-evaluation-based frameworks (Figure 1 (b)). These methods quantitatively assess candidate trajectories in terms of collision risk, lane departure, and driving comfort, providing scene-level safety evaluations before selecting the final driving plan. While these approaches are effective for ensuring safety at a coarse level, their reasoning remains largely implicit. They evaluate safety by scoring entire trajectories based on global scene representations, without explicitly modeling why a trajectory is safe or under what specific conditions safety may be compromised. As a result, they overlook fine-grained safety, which requires explicit reasoning over surrounding agents, temporal dependencies, and localized risk dynamics. Due to this limitation, such models struggle to accurately distinguish trajectories that may lead to collisions when small deviations occur in complex interaction scenarios.

Another line of research [22, 35, 43, 47–49] explores world-model rollouts, which simulate the evolution of a scene in response to the ego vehicle’s future actions (see Figure 1(a)). These approaches predict how the environment may unfold across multiple plausible futures, allowing autonomous systems to anticipate complex traffic situations and support safety-critical decision making. Beyond simple future prediction, world models simulate latent scene evolution to construct a coherent world representation for robust planning and reasoning. Previous methods implement this paradigm using dense spatial representations, such as occupancy-based [35, 43, 49] or BEV-based [22, 47] world models, to simulate scene evolution under various hypothetical scenarios. However, dense scene representations

are often insufficient for capturing complex risk factors that emerge from dynamic interactions among agents. Since these representations describe the environment in a grid-centric manner, they lack explicit mechanisms to model the relational dynamics between the ego agent and potential risk factors, ultimately limiting their ability to perform safety-critical reasoning.

To address these challenges, we introduce a novel end-to-end driving framework, referred to as SafeDrive. As illustrated in Figure 1 (c), SafeDrive distinguishes itself from existing end-to-end planning approaches by introducing a sparse world model designed for instance-level interaction and safety reasoning. To realize this design, we propose two primary modules: the Sparse World Network (SWNet) and the Fine-grained Reasoning Network (FRNet).

SWNet employs Sparse World Model that constructs ego-trajectory-conditioned sparse world representations to simulate plausible future state evolutions of a finite set of entities within a scene. Unlike previous world models that generate dense scene representations, our Sparse World Model focuses on key dynamic agents and essential road elements. This enables the model to predict the future behaviors of critical scene components and explicitly capture their interactive dynamics with the ego agent, conditioned on the ego’s motion. During simulation, the predicted motions of the ego and surrounding agents are jointly refined, ensuring mutual consistency between their behaviors. To model these pair-wise inter-agent interactions, we employ a self-attention mechanism that allows information exchange across all dynamic agents in the scene.

Using future states spanned by the Sparse World Model, FRNet can effectively assess the safety of a given ego trajectory plan. Most existing approaches estimate safety scores by encoding the ego trajectory together with the entire scene representation. While this holistic approach simplifies the formulation, it places the burden on the model to determine which aspects of the scene are relevant for safety evaluation, which could limit the accuracy. To overcome this limitation, we introduce a fine-grained safety reasoning that enables more precise and interpretable safety assessment.

To design this framework, we draw inspiration from how human drivers respond to potential future risks. When facing a risky situation, a human driver first identifies the relevant agents that could potentially lead to a collision and then evaluates which driving plan would be most appropriate based on the anticipated future behaviors of those agents. Motivated by this observation, we propose a collision assessment framework that estimates collision risk in a pair-wise manner between the ego agent and each dynamic agent in the scene. The model predicts the likelihood of contact for every agent at each future timestep, allowing it to reason precisely about when and how potential collisions may occur. By restricting the model’s role to evaluating

pair-wise collision risks between interacting agents, our approach achieves a more accurate and rigorous safety analysis.

In parallel, we introduce a complementary safety reasoning module that evaluates drivable area compliance. By leveraging road entities represented in the Sparse World Model, this module predicts the spatial and temporal points at which the ego agent may violate road boundaries or lane constraints. Together, these mechanisms enable FRNet to deliver detailed, interpretable, and temporally grounded safety assessments.

We evaluate SafeDrive on both the open-loop NAVSIM and the closed-loop Bench2Drive benchmarks. On the real-world NAVSIM dataset, SafeDrive achieves a PDMS of 91.6 and an EPDMS of 87.5, corresponding to only 61 collisions across 12,146 scenes (0.5%), establishing a new state of the art in safety-critical planning performance. In the closed-loop Bench2Drive simulation, SafeDrive attains a 66.8% driving score, demonstrating strong robustness and stability under interactive driving conditions that require real-world decision making.

The contributions of this study are summarized below:

- We present SafeDrive, an end-to-end planning framework that leverages a sparse world model to perform fine-grained, instance-level safety reasoning for reliable driving decisions.
- We introduce SWNet, which constructs trajectory-conditioned sparse worlds and models the structural relationships among scene entities, serving as a foundation for interpretable instance-level safety reasoning.
- We propose FRNet that explicitly models pair-wise collision risks and time-wise lane adherence, enabling fine-grained safety assessment grounded in instance-level interactions.
- Extensive evaluations on both open-loop (NAVSIM) and closed-loop (Bench2Drive) benchmarks verify the superior robustness and reliability of SafeDrive under diverse and safety-critical driving scenarios.
- We will release the code publicly.

2. Related Works

2.1. End-to-End Planning

End-to-end autonomous driving mitigates error propagation in modular pipelines by integrating perception, prediction, and planning within a unified model. UniAD [9] established this paradigm with a query-based sequential transformer, leading to improvements in efficiency and scalability through parallelized architectures [12, 38] and compact scene representations [13, 34]. To ensure safety under diverse real-world conditions, recent approaches incorporate trajectory evaluation mechanisms. Hydra-MDP [17, 23] introduces rule-based signals such as lane-keeping, traffic-

light compliance, and comfort to guide trajectory selection. DriveSuprim [44] employs multi-stage scoring and data augmentation to improve generalization.

2.2. World Model for Autonomous Driving

World models in autonomous driving, which predict future states conditioned on the ego vehicle’s actions, have progressed along two main directions. One direction focuses on generating realistic future scenarios in video form [6, 8, 10, 20, 36, 37] for simulation-based planner validation or data augmentation. The second direction aims to integrate predictive scene understanding into the planning process, thereby enhancing interaction reasoning and safety-aware planning [18, 21, 22, 28, 47, 49]. OccWorld [49] and DriveWorld [28] model action-conditioned scene evolution in a 4D occupancy space, providing temporally consistent geometry for end-to-end planning. LAW [21] and SSR [18] improve planning performance by self-supervising the evolution of latent future representations. WoTE [22] predicts future BEV states and utilizes them to enhance trajectory evaluation and safety assessment reliability.

3. Method

3.1. Overview

The overall architecture of SafeDrive is illustrated in Figure 2. SafeDrive consists of three core modules: ProposalNet, SWNet, and FRNet. ProposalNet first preprocesses the input sensor data to generate the object queries, BEV features, and planning queries required for subsequent sparse world construction. SWNet then builds a Sparse World, where each planning query constructs a trajectory-conditioned world that simulates the scene’s evolution with surrounding instances. Through this sparse formulation, SWNet focuses on safety-critical instances and encodes their relational representations, establishing a structured basis for fine-grained safety reasoning. Finally, FRNet determines the most feasible and safety-consistent driving trajectory through fine-grained reasoning over these interaction-aware representations, assessing potential risks such as pair-wise collisions and lane departures.

3.2. ProposalNet

The ProposalNet encodes multi-modal sensor inputs into a unified BEV feature map and detects surrounding instances that may affect the ego’s motion. It then evaluates the coarse safety and feasibility of trajectory anchors at the scene level and filters out unsafe or infeasible ones, producing a compact set of safety-aware trajectory candidates for constructing sparse worlds.

BEV Encoder. ProposalNet generates spatio-temporal BEV features by processing multi-modal data captured by

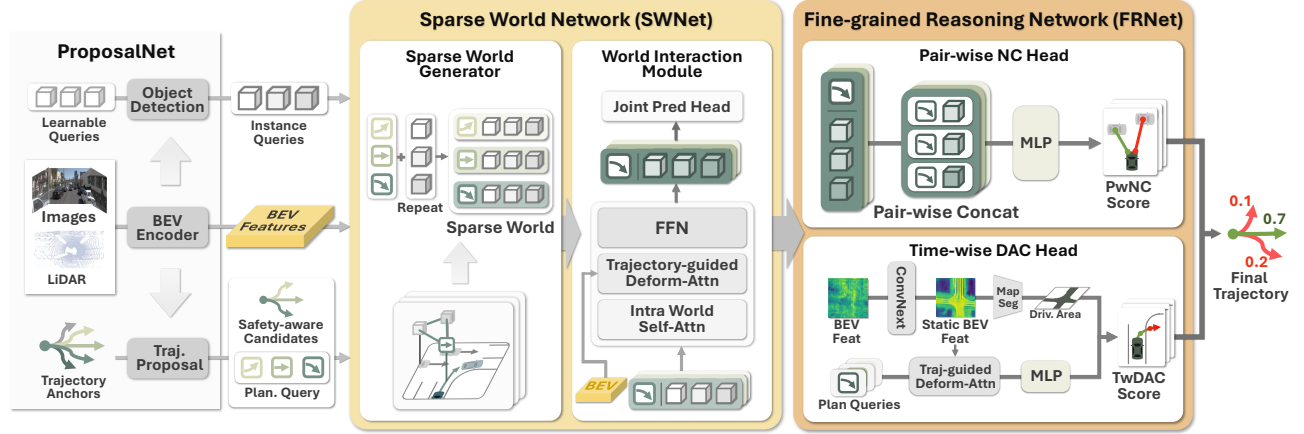


Figure 2. **Overall architecture of SafeDrive.** ProposalNet evaluates the scene-level safety of anchor trajectories using BEV features and selects safety-aware candidates. SWNet constructs trajectory-conditioned Sparse Worlds by simulating the future behaviors of dynamic agents and road entities. FRNet performs fine-grained safety reasoning by estimating pair-wise No at-fault Collision score and evaluating Time-wise Drivable Area Compliance score over time, enabling interpretable and temporally grounded safety assessment.

cameras and LiDAR sensors. Image features are extracted using a backbone network such as ResNet-34 [7], while LiDAR point clouds are encoded into BEV representations through voxel encoding [42]. Following the BEVFormer-M [24], learnable BEV queries fuse the two modalities into a unified BEV map by attending to both image and LiDAR features. To encode temporal context, BEV features from previous timesteps are concatenated with the current feature and passed through a convolutional layer to generate spatio-temporal BEV features F_{BEV} .

Object Detection. Learnable object queries extract instance-level representations from BEV features using deformable attention [24] and are decoded into instance queries. The updated instance representations are then used to estimate the centroids, headings, classification scores, and motion states of surrounding instances. The detected instance queries are filtered according to a classification score threshold, and the remaining queries $\mathcal{O}_{\text{ins}} = \{o_{\text{ins}}^i\}_{i=1}^N$ together with their motion trajectories $\mathcal{T}_{\text{ins}} = \{\tau_{\text{ins}}^i\}_{i=1}^N$ are used to construct the sparse world, where N denotes the number of instances.

Trajectory Candidate Generation. We define trajectory anchors $\mathcal{A} = \{A^j\}_{j=1}^K$ obtained via K-means clustering on ego trajectories from the training dataset, where K denotes the number of anchors. These anchors are embedded through an MLP, producing the planning queries $\mathcal{Q}_{\text{plan}} = \{q_{\text{plan}}^j\}_{j=1}^K$. To capture spatio-temporal scene context along the trajectories associated with each planning query, we extend the standard 2D deformable attention [50] into a *trajectory-guided deformable attention* that samples BEV

features F_{BEV} along the trajectories and integrates them through a feed-forward network (FFN):

$$\hat{\mathcal{Q}}_{\text{plan}} = \text{FFN}(\text{Deform-Attn}_{\text{traj}}(\mathcal{Q}_{\text{plan}}, \mathcal{A}, F_{\text{BEV}})). \quad (1)$$

The decoded planning queries $\hat{\mathcal{Q}}_{\text{plan}}$ are then passed through MLP heads to predict refined trajectories, an imitation score, and scene-level safety scores based on five criteria: no at-fault collisions (NC), drivable area compliance (DAC), time-to-collision (TTC), comfort (C), and ego progress (EP). The overall score of the ProposalNet is computed as a weighted log-sum of the imitation and safety terms, and the top- K' trajectories are selected as the safety-aware candidate query features $\mathcal{C}_{\text{plan}} = \{c_{\text{plan}}^j\}_{j=1}^{K'}$ with their corresponding trajectories $\mathcal{T}_{\text{plan}} = \{\tau_{\text{plan}}^j\}_{j=1}^{K'}$.

3.3. Sparse World Network (SWNet)

SWNet consists of two components: the Sparse World Generator and the World Interaction Module. The Sparse World Generator constructs a Sparse World for each safety-aware candidate trajectory by combining it with the surrounding instances. The World Interaction Module models trajectory-conditioned interactions between the ego vehicle and its surrounding instances, jointly refining their future motions within the same world.

Sparse World Generator. To construct Sparse Worlds for each safety-aware candidate query, the instance queries \mathcal{O}_{ins} and their motion trajectories \mathcal{T}_{ins} are repeated K' times and concatenated with the corresponding safety-aware candidate queries $\mathcal{C}_{\text{plan}}$, resulting in the sparse world set $\mathcal{W} = \{c_{\text{plan}}^j, o_{\text{ins}}^1, \dots, o_{\text{ins}}^N\}_{j=1}^{K'}$ and their corresponding trajectory set $\mathcal{T}_{\text{world}} = \{\tau_{\text{plan}}^j, \tau_{\text{ins}}^1, \dots, \tau_{\text{ins}}^N\}_{j=1}^{K'}$.

World Interaction Module. The World Interaction Module enhances each Sparse World by modeling detailed interactions among the ego trajectory and surrounding instances. It first applies intra-world self-attention to capture relational dependencies between trajectory and instance queries, and then performs trajectory-guided deformable attention, which follows the same structure as Eq. 1, to aggregate spatio-temporal features from F_{BEV} along each candidate trajectory and the predicted future positions of nearby instances:

$$\begin{aligned}\bar{\mathcal{W}} &= \text{World-SelfAttn}(\mathcal{W}), \\ \hat{\mathcal{W}} &= \text{FFN}(\text{Deform-Attn}_{\text{traj}}(\bar{\mathcal{W}}, \mathcal{T}_{\text{world}}, F_{\text{BEV}})).\end{aligned}\quad (2)$$

Leveraging these trajectory-conditioned interactions, the module jointly refines the candidate trajectories and the future motions of surrounding instances. The resulting refined world set $\hat{\mathcal{W}} = \{\hat{c}_{\text{plan}}^j, \hat{o}_{\text{ins}}^{1,j}, \dots, \hat{o}_{\text{ins}}^{N,j}\}_{j=1}^{K'}$ and the refined planning trajectory set $\hat{\mathcal{T}}_{\text{plan}} = \{\hat{\tau}_{\text{plan}}^j\}_{j=1}^{K'}$ are delivered to FRNet for fine-grained safety reasoning.

3.4. Fine-grained Reasoning Network (FRNet)

FRNet determines the final driving trajectory through fine-grained safety assessment, utilizing interaction-aware representations from SWNet. Specifically, it computes two safety metrics for each candidate trajectory: the Pair-wise No at-fault Collision (PwNC) and Time-wise Drivable Area Compliance (TwDAC).

(i) Pair-wise No at-fault Collision. The PwNC metric evaluates the ego vehicle’s interaction safety with surrounding instances by estimating the probability of maintaining safe and non-conflicting motion patterns over future timesteps. To compute this metric, each trajectory query is paired with the instance queries within the same world through concatenation, producing plan–instance pair-wise features $\{[\hat{c}_{\text{plan}}^j, \hat{o}_{\text{ins}}^{1,j}], \dots, [\hat{c}_{\text{plan}}^j, \hat{o}_{\text{ins}}^{N,j}]\}_{j=1}^{K'}$. Building upon the interaction-aware representations established by SWNet, these pairwise features capture how each surrounding instance dynamically interacts with the ego vehicle’s planned motion within the shared world context. The features are then passed through an MLP f_{pwnc} followed by a sigmoid activation σ to produce PwNC scores:

$$p_{\text{pwnc}}^{i,j} = \sigma(f_{\text{pwnc}}([\hat{c}_{\text{plan}}^j, \hat{o}_{\text{ins}}^{i,j}])), \quad (3)$$

where $p_{\text{pwnc}}^{i,j} \in [0, 1]^H$ represents the probability that the j -th planned trajectory remains collision-free with the i -th surrounding instance over the future horizon H . The overall PwNC score P_{PwNC}^j for the j -th trajectory candidate is obtained by multiplying the per-instance PwNC scores over all instances and timesteps:

$$P_{\text{PwNC}}^j = \prod_{i=1}^N \prod_{h=1}^H p_{\text{pwnc}}^{i,j}(h). \quad (4)$$

(ii) Time-wise Drivable Area Compliance. To evaluate whether each candidate trajectory stays within drivable regions over time, we compute TwDAC scores from BEV representations. Since the BEV features F_{BEV} contain both dynamic and static information, we apply a ConvNeXt-v2 [39] block with a lightweight segmentation head to produce static BEV segmentation maps (e.g., drivable areas and lane centerlines) and extract intermediate features $F_{\text{BEV}}^{\text{static}}$ as spatial priors for drivable-area reasoning. Trajectory-guided deformable attention is then performed over $F_{\text{BEV}}^{\text{static}}$ using the refined future positions $\hat{\mathcal{T}}_{\text{plan}}$ as reference points, and TwDAC scores are predicted via an MLP f_{twdac} with a sigmoid activation:

$$\begin{aligned}\bar{c}_{\text{plan}}^j &= \text{Deform-Attn}_{\text{traj}}(\hat{c}_{\text{plan}}^j, \hat{\tau}_{\text{plan}}^j, F_{\text{BEV}}^{\text{static}}), \\ p_{\text{twdac}}^j &= \sigma(f_{\text{twdac}}(\bar{c}_{\text{plan}}^j)),\end{aligned}\quad (5)$$

where $p_{\text{twdac}}^j \in [0, 1]^H$ represents the TwDAC scores of the j -th planned trajectory over the future horizon H .

Fine-grained boundary transitions near drivable-area boundaries are inherently difficult to capture with precision. To mitigate this issue, we sample the drivable-area probability map M_{Driv} from the predicted BEV segmentation map at nine key points of each future ego box (center, corners, and edge midpoints). The final TwDAC score of the j -th planning query is computed by multiplying all sampled probabilities across timesteps and sampled points:

$$P_{\text{TwDAC}}^j = \prod_{h=1}^H \left(p_{\text{twdac}}^j(h) \times \prod_{k=1}^9 M_{\text{Driv}}^j(h, k) \right), \quad (6)$$

where $M_{\text{Driv}}^j(h, k)$ represents the drivable-area probability sampled via bilinear interpolation at the k -th location among the nine key points of the j -th planning query’s ego box at timestep h .

(iii) Safety Integration and Trajectory Selection. To determine the final driving plan, FRNet integrates the fine-grained safety metrics with the scene-level evaluations of each candidate trajectory to produce a unified safety assessment. Given the refined planning queries from SWNet, we predict planning-related terms such as imitation score, EP, C, and TTC through lightweight MLP heads. These estimates are combined with PwNC and TwDAC via a weighted log-sum in the log-probability space to obtain an overall safety score for each candidate. The trajectory with the highest score is then selected as the final driving plan.

3.5. Loss Function

The overall training loss of SafeDrive is defined as a weighted sum of task-specific objectives:

$$\begin{aligned}\mathcal{L}_{\text{total}} &= \lambda_1 \mathcal{L}_{\text{det-motion}} + \lambda_2 \mathcal{L}_{\text{seg}} + \lambda_3 \mathcal{L}_{\text{plan}} \\ &\quad + \lambda_4 \mathcal{L}_{\text{PwNC}} + \lambda_5 \mathcal{L}_{\text{TwDAC}} + \lambda_6 \mathcal{L}_{\text{SL-safety}}.\end{aligned}\quad (7)$$

Table 1. **Evaluation of PDMS performance on the NAVSIM dataset.** "C" and "L" denote Camera and LiDAR inputs, respectively. The best and second-best results are highlighted in bold and underline, respectively. Unless noted, models use ResNet-34 as the image backbone, and "†" marks the one using V2-99. The "-" denotes that the associated results are not available.

| Method | Venue | Input | NC | DAC | TTC | EP | Comfort | PDMS |
|-------------------------|--------------|-------|-------------|-------------|-------------|-------------|-------------|-------------|
| Human | - | - | 100.0 | 100.0 | 100.0 | 87.5 | 99.9 | 94.8 |
| UniAD [9] | CVPR 2023 | C | 97.8 | 91.9 | 92.9 | 78.8 | 100 | 83.4 |
| Transfuser [29] | CVPR 2021 | C&L | 97.7 | 92.8 | 92.8 | 79.2 | 100 | 84.0 |
| PARA-Drive [38] | CVPR 2024 | C | 97.9 | 92.4 | 93.0 | 79.3 | 99.8 | 84.0 |
| LAW [21] | ICLR 2025 | C | 96.4 | 95.4 | 88.7 | 81.7 | <u>99.9</u> | 84.6 |
| DistillDrive [45] | ICCV 2025 | C&L | 98.1 | 94.6 | 93.6 | 81.0 | 100 | 86.2 |
| Hydra-MDP [23] | arXiv 2024 | C&L | 98.3 | 96.0 | 94.6 | 78.7 | 100 | 86.5 |
| DiffusionDrive [26] | CVPR 2025 | C&L | 98.2 | 96.2 | 94.7 | 82.2 | 100 | 88.1 |
| WoTE [22] | ICCV 2025 | C&L | <u>98.5</u> | 96.8 | <u>94.9</u> | 81.9 | <u>99.9</u> | 88.3 |
| GaussianFusion [27] | NeurIPS 2025 | C&L | 98.3 | 97.2 | 94.6 | 83.0 | - | 88.8 |
| SeerDrive [47] | NeurIPS 2025 | C&L | 98.4 | 97.0 | <u>94.9</u> | 83.2 | <u>99.9</u> | 88.9 |
| GoalFlow† [41] | CVPR 2025 | C&L | 98.4 | <u>98.3</u> | 94.6 | 85.0 | 100 | <u>90.3</u> |
| SafeDrive (Ours) | - | C&L | 99.5 | 99.0 | 97.2 | <u>84.3</u> | 100 | 91.6 |

Table 2. **Evaluation of EPDMS performance on the NAVSIM dataset.** "C" and "L" denote Camera and LiDAR inputs, respectively. All methods use a ResNet-34 backbone for a fair comparison. Methods marked with "*" are reproduced from released checkpoints.

| Method | Venue | Input | NC | DAC | DDC | TLC | EP | TTC | LK | HC | EC | EPDMS |
|-------------------------|--------------|-------|-------------|-------------|-------------|-------------|-------------|-------------|-------------|-------------|-------------|-------------|
| Hydra-MDP++ [17] | arXiv 2025 | C | 97.2 | <u>97.5</u> | 99.4 | 99.6 | 83.1 | 96.5 | 94.4 | <u>98.2</u> | 70.9 | 81.4 |
| DriveSuprim [44] | arXiv 2025 | C | 97.5 | 96.5 | 99.4 | 99.6 | <u>88.4</u> | 96.6 | 95.5 | 98.3 | 77.0 | 83.1 |
| WoTE* [22] | ICCV 2025 | C&L | <u>98.5</u> | 96.8 | 98.8 | <u>99.8</u> | 86.0 | <u>97.9</u> | 95.4 | 98.3 | <u>83.0</u> | 84.1 |
| DiffusionDrive* [26] | CVPR 2025 | C&L | 98.2 | 96.2 | <u>99.5</u> | <u>99.8</u> | 87.4 | 97.4 | 97.0 | 98.3 | 87.8 | 84.8 |
| GaussianFusion [27] | NeurIPS 2025 | C&L | 98.3 | 97.3 | 99.0 | 97.4 | 87.5 | 97.4 | <u>97.4</u> | 98.3 | - | <u>85.0</u> |
| SafeDrive (Ours) | - | C&L | 99.5 | 99.0 | 99.7 | 99.9 | 88.6 | 98.9 | 97.5 | <u>98.2</u> | 81.9 | 87.5 |

where each coefficient λ_i adjusts the relative contribution of its corresponding component. $\mathcal{L}_{\text{det-motion}}$ is applied to detection, classification, and motion prediction of surrounding instances, and \mathcal{L}_{seg} is used for BEV segmentation of static map elements such as drivable areas and lane centerlines. $\mathcal{L}_{\text{plan}}$ supervises the prediction of imitation scores and the refinement of candidate trajectories based on expert driving behaviors. $\mathcal{L}_{\text{PwNC}}$ and $\mathcal{L}_{\text{TwDAC}}$ supervise FRNet’s estimation of the fine-grained safety scores PwNC and TwDAC. Finally, $\mathcal{L}_{\text{SL-safety}}$ covers the scene-level safety terms in ProposalNet and SWNet, including NC, DAC, EP, C, and TTC.

4. Experiments

4.1. Dataset & Metrics

To comprehensively evaluate our method, we conducted both open-loop and closed-loop evaluations using two benchmarks.

NAVSIM (Open-loop Evaluation). NAVSIM [5] is a real-world, planning-oriented benchmark built upon *OpenScene* [4], a compact redistribution of *nuPlan* [14]. It provides 360° perception from eight cameras and five LiDARs with 2 Hz annotations that include HD maps and bounding boxes, focusing on complex intention-changing scenarios

while excluding trivial stationary ones. We trained and evaluated our model on the official *navtrain* (103k) and *navtest* (12k) splits. For evaluation, NAVSIM adopts closed-loop-derived metrics to assess open-loop safety and fidelity: the PDM Score (PDMS) and its extended version (EPDMS). The PDM Score (PDMS) integrates five criteria (NC, DAC, TTC, EP, and C), and its extended version (EPDMS) additionally includes Driving Direction Compliance (DDC), Traffic Light Compliance (TLC), Lane Keeping (LK), History Comfort (HC), and Extended Comfort (EC).

Bench2Drive (Closed-loop Evaluation). Bench2Drive [11] is a CARLA-based benchmark containing 220 safety-critical driving routes across all towns. The dataset is collected from the expert model Think2Drive [19], comprising 1,000 clips (950 for training and 50 for testing). It evaluates closed-loop performance using two key metrics: Success Rate and Driving Score. Details of the NAVSIM and Bench2Drive metrics are provided in the Appendix.

4.2. Implementation Details

SafeDrive employs ResNet-34 [7] as the image backbone and SECOND [42] as the LiDAR backbone, and adopts BEVFormer-M [24] as the BEV encoder. This design choice aims to obtain high-quality detection and

Table 3. Closed-loop Results on Bench2Drive Benchmark

| Method | Venue | DS | SR(%) |
|-------------------------|--------------|--------------|--------------|
| TCP [40] | NeurIPS 2022 | 40.70 | 15.00 |
| VAD [13] | ICCV 2023 | 42.35 | 15.00 |
| UniAD-Base [9] | CVPR 2023 | 45.81 | 16.36 |
| BridgeAD [46] | CVPR 2025 | 50.06 | 22.73 |
| Hydra-MDP [23] | arXiv 2024 | 59.95 | 29.82 |
| WoTE [22] | ICCV 2025 | 61.71 | 31.36 |
| DriveDPO [31] | NeurIPS 2025 | 62.02 | 30.62 |
| DriveTransformer [12] | ICLR 2025 | <u>63.46</u> | <u>35.01</u> |
| SafeDrive (Ours) | - | 66.77 | 42.40 |

BEV segmentation performance, which is essential for fine-grained reasoning. In comparison, the Transfuser [29] BEV backbone provides lower performance on these tasks. The number of camera views is 3 for NAVSIM and 4 for Bench2Drive, with image resolutions of 256×512 and 576×1024, respectively. The number of trajectory anchors K is initialized to 256, and the number of candidate trajectories K' is 128. ProposalNet and SWNet consist of two and four decoding layers, respectively. The planning horizon is 4 seconds (8 future steps) for NAVSIM and 3 seconds (6 steps) for Bench2Drive. For both benchmarks, the model was first pretrained on object detection and BEV segmentation, followed by full end-to-end training. Additional training details are provided in the Appendix.

4.3. Performance Comparison

Results on NAVSIM. Table 1 summarizes the performance of SafeDrive on the NAVSIM test benchmark using the PDMS metric. SafeDrive significantly outperforms previous state-of-the-art methods [9, 21–23, 26, 27, 29, 38, 41, 45], achieving a SOTA performance with a PDMS of 91.6. Notably, its fine-grained safety reasoning yields an NC score of 99.5, corresponding to only 61 collisions out of 12,146 test cases, and a DAC score of 99.0, indicating high adherence to drivable-area constraints. Table 2 reports the 87.5 EPDMS results, where SafeDrive achieves the highest overall performance.

Results on Bench2Drive. Table 3 presents the closed-loop evaluation results of several end-to-end autonomous driving methods [9, 12, 13, 22, 23, 31, 40, 46] on the Bench2Drive benchmark. The proposed SafeDrive demonstrates performance improvements compared to existing approaches. SafeDrive surpasses the current leading method, DriveTransformer [12], by 3.31 points in Driving Score, demonstrating that our model achieves consistent and robust driving performance across diverse scenarios.

4.4. Ablation Study

Contribution of Main Components. Table 4 summarizes the contribution of each SafeDrive component. Due

Table 4. Ablation study for evaluating the main components. "Diff" denotes the DiffusionDrive [26] head, "Prop" indicates the ProposalNet, and "SL Eval" refers to the scene-level safety evaluation.

| Diff | Prop | SL Eval | SWNet | FRNet | NC | DAC | TTC | EP | PDMS |
|------|------|---------|-------|-------|-------------|-------------|-------------|-------------|-------------|
| ✓ | | | | | 98.8 | 96.3 | 82.3 | 95.8 | 88.6 |
| | ✓ | | | | 98.9 | 97.1 | 95.1 | 83.2 | 89.1 |
| | ✓ | ✓ | | | 99.0 | 97.7 | 96.3 | 83.5 | 90.1 |
| | ✓ | ✓ | ✓ | | 99.2 | 98.2 | 96.7 | 84.4 | 90.9 |
| | ✓ | ✓ | | ✓ | 99.2 | 98.5 | 96.0 | 84.6 | 90.9 |
| ✓ | ✓ | ✓ | ✓ | ✓ | 99.5 | 99.0 | 97.2 | 84.3 | 91.6 |

Table 5. Ablation study on world representation

| World Representation | Fine-grained Safety | NC | DAC | TTC | PDMS |
|----------------------|---------------------|-------------|-------------|-------------|-------------|
| No | ✓ | 99.2 | 98.5 | 96.0 | 90.9 |
| BEV | | 98.8 | 98.0 | 95.5 | 90.3 |
| BEV | ✓ | 99.2 | 98.3 | 96.5 | 90.9 |
| Sparse | | 99.2 | 98.2 | 96.7 | 90.9 |
| Sparse | ✓ | 99.5 | 99.0 | 97.2 | 91.6 |

Table 6. Ablation study on the impact of PwNC and TwDAC

| PwNC | TwDAC | NC | DAC | TTC | PDMS |
|------|-------|-------------|-------------|-------------|-------------|
| | | 99.2 | 98.5 | 96.0 | 90.9 |
| ✓ | | 99.5 | 98.7 | 97.3 | 91.5 |
| | ✓ | 99.2 | 99.0 | 96.7 | 91.4 |
| ✓ | ✓ | 99.5 | 99.0 | 97.2 | 91.6 |

to the effects of proposed trajectory-guided deformable attention, replacing the DiffusionDrive [26] head with ProposalNet yields a 0.5 PDMS improvement. Introducing scene-level safety on top of this results in an additional gain of 1.0 PDMS. Adding SWNet and FRNet yields performance gains of 0.8 each. Finally, adding both SWNet and FRNet yields an additional 0.7 gain, showing that sparse-world instance-level interactions are essential for fine-grained safety reasoning and safe driving behavior.

Effect of the World Representation. Table 5 presents the performance of different world-model representations when fine-grained safety evaluation is applied. Sparse World surpasses BEV World [22] by 0.6 PDMS. While BEV cannot capture instance-level interactions or fine-grained safety, and thus fails to benefit from fine-grained reasoning, Sparse World supports these checks and yields an additional 0.7 PDMS gain.

Fine-Grained Safety Reasoning. Table 9 presents the experimental results of using PwNC and TwDAC scores within FRNet. PwNC and TwDAC individually provide 0.6 and 0.5 performance improvements, respectively, and using them together yields a 0.7 improvement.

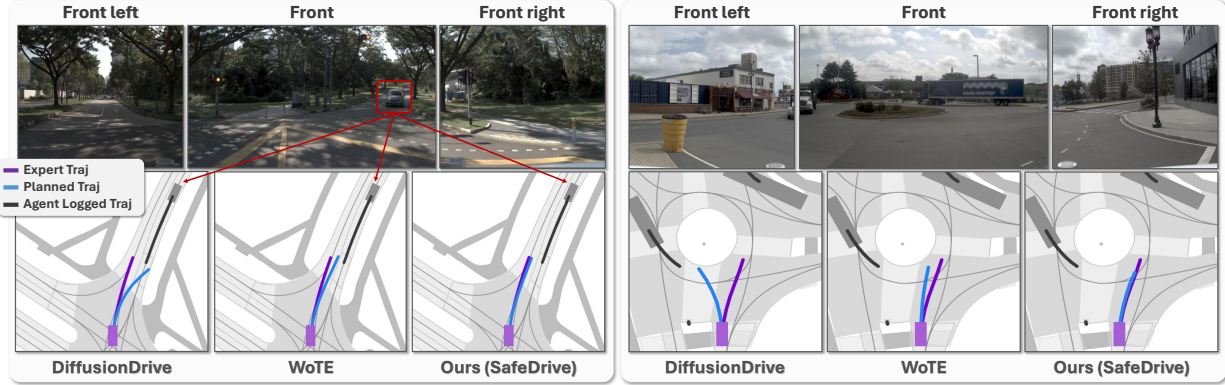


Figure 3. **Qualitative comparison with other SOTA models on the NAVSIM test set.** The expert trajectory (GT) is shown in purple, the predicted trajectories of each model are shown in blue, and the log-replayed future trajectories of surrounding agents are shown in black.

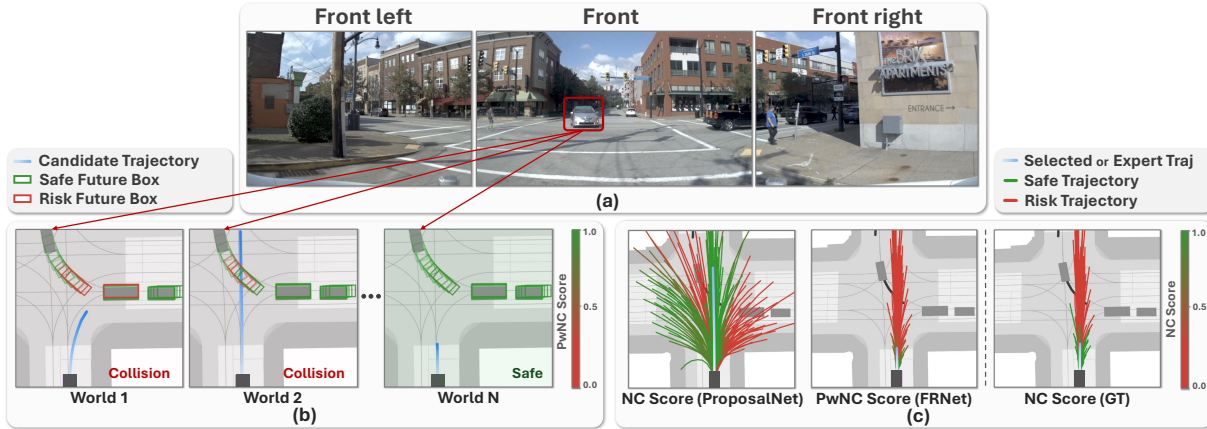


Figure 4. **Visualization of the PwNC-based reasoning process.** (a) Current scene images. (b) Predicted PwNC values are used to color-shade the logged future positions of surrounding vehicles. (c) NC-score visualization of all candidate trajectories for GT, ProposalNet, and FRNet. Green for surrounding-vehicle boxes and candidate trajectories indicates higher safety, while red denotes elevated risk.

4.5. Qualitative Results

Qualitative results compared with SOTA models. Figure 3 illustrates the qualitative results generated by the proposed SafeDrive. We compare our method with the state-of-the-art methods [22, 26], and SafeDrive generates trajectories of higher fidelity compared to other models.

Qualitative analysis of the reasoning process for PwNC. Figure 4 illustrates the fine-grained reasoning process of SafeDrive using PwNC. As shown in Figure 4 (b), the trajectory assigned the highest score by ProposalNet results in a collision. FRNet evaluates the candidate trajectories using the predicted collision likelihood and timing (PwNC) and, through fine-grained reasoning, selects a safe alternative trajectory. These visualizations demonstrate that SafeDrive effectively performs interpretable and safety-oriented decision making.

5. Conclusion

In this paper, we presented **SafeDrive**, an end-to-end autonomous driving framework that integrates sparse world modeling with explicit, fine-grained safety reasoning. SafeDrive introduces the SWNet that constructs trajectory-conditioned worlds, enabling instance-level interaction modeling among dynamic agents and road entities. Built upon these interaction-centric representations, the FRNet performs detailed safety assessment through pairwise collision analysis and time-wise drivable-area compliance evaluation. By jointly modeling future interactions and evaluating safety at multiple levels of granularity, SafeDrive produces planning decisions that are reliable even in complex and dynamic environments. Extensive experiments on both the open-loop NAVSIM and closed-loop Bench2Drive benchmarks demonstrate that SafeDrive achieves state-of-the-art safety performance and robust driving behavior under complex real-world scenarios.

References

- [1] Shaoyu Chen, Bo Jiang, Hao Gao, Bencheng Liao, Qing Xu, Qian Zhang, Chang Huang, Wenyu Liu, and Xinggong Wang. Vadv2: End-to-end vectorized autonomous driving via probabilistic planning. *arXiv preprint arXiv:2402.13243*, 2024. 2
- [2] Xuesong Chen, Linjiang Huang, Tao Ma, Rongyao Fang, Shaoshuai Shi, and Hongsheng Li. Solve: Synergy of language-vision and end-to-end networks for autonomous driving. In *Proceedings of the IEEE/CVF Conference on Computer Vision and Pattern Recognition 2025*. IEEE, 2025. 14
- [3] Zhili Chen, Maosheng Ye, Shuangjie Xu, Tongyi Cao, and Qifeng Chen. Ppad: Iterative interactions of prediction and planning for end-to-end autonomous driving. In *European Conference on Computer Vision*, pages 239–256. Springer, 2024. 2
- [4] OpenScene Contributors. Openscene: The largest up-to-date 3d occupancy prediction benchmark in autonomous driving. <https://github.com/OpenDriveLab/OpenScene>, 2023. 6
- [5] Daniel Dauner, Marcel Hallgarten, Tianyu Li, Xinshuo Weng, Zhiyu Huang, Zetong Yang, Hongyang Li, Igor Gilitschenski, Boris Ivanovic, Marco Pavone, et al. Navsim: Data-driven non-reactive autonomous vehicle simulation and benchmarking. *Advances in Neural Information Processing Systems*, 37:28706–28719, 2024. 6, 13
- [6] Shenyuan Gao, Jiazhi Yang, Li Chen, Kashyap Chitta, Yihang Qiu, Andreas Geiger, Jun Zhang, and Hongyang Li. Vista: A generalizable driving world model with high fidelity and versatile controllability. *Advances in Neural Information Processing Systems*, 37:91560–91596, 2024. 3
- [7] Kaiming He, Xiangyu Zhang, Shaoqing Ren, and Jian Sun. Deep residual learning for image recognition. In *Proceedings of the IEEE Conference on Computer Vision and Pattern Recognition*, pages 770–778, 2016. 4, 6
- [8] Anthony Hu, Lloyd Russell, Hudson Yeo, Zak Murez, George Fedoseev, Alex Kendall, Jamie Shotton, and Gianluca Corrado. Gaia-1: A generative world model for autonomous driving. *arXiv preprint arXiv:2309.17080*, 2023. 3
- [9] Yihan Hu, Jiazhi Yang, Li Chen, Keyu Li, Chonghao Sima, Xizhou Zhu, Siqi Chai, Senyao Du, Tianwei Lin, Wenhai Wang, et al. Planning-oriented autonomous driving. In *Proceedings of the IEEE/CVF Conference on Computer Vision and Pattern Recognition*, pages 17853–17862, 2023. 2, 3, 6, 7
- [10] Fan Jia, Weixin Mao, Yingfei Liu, Yucheng Zhao, Yuqing Wen, Chi Zhang, Xiangyu Zhang, and Tiancai Wang. Adriver-i: A general world model for autonomous driving. *arXiv preprint arXiv:2311.13549*, 2023. 3
- [11] Xiaosong Jia, Zhenjie Yang, Qifeng Li, Zhiyuan Zhang, and Junchi Yan. Bench2drive: Towards multi-ability benchmarking of closed-loop end-to-end autonomous driving. *Advances in Neural Information Processing Systems*, 37:819–844, 2024. 6, 13
- [12] Xiaosong Jia, Junqi You, Zhiyuan Zhang, and Junchi Yan. Drivetransformer: Unified transformer for scalable end-to-end autonomous driving. *arXiv preprint arXiv:2503.07656*, 2025. 2, 3, 7
- [13] Bo Jiang, Shaoyu Chen, Qing Xu, Bencheng Liao, Jiajie Chen, Helong Zhou, Qian Zhang, Wenyu Liu, Chang Huang, and Xinggong Wang. Vad: Vectorized scene representation for efficient autonomous driving. In *Proceedings of the IEEE/CVF International Conference on Computer Vision*, pages 8340–8350, 2023. 2, 3, 7
- [14] Napat Karnchanachari, Dimitris Geromichalos, Kok Seang Tan, Nanxiang Li, Christopher Eriksen, Shakiba Yaghoubi, Noushin Mehdipour, Gianmarco Bernasconi, Whye Kit Fong, Yiluan Guo, et al. Towards learning-based planning: The nuPlan benchmark for real-world autonomous driving. In *2024 IEEE International Conference on Robotics and Automation (ICRA)*, pages 629–636. IEEE, 2024. 6
- [15] Diederik P. Kingma and Jimmy Ba. Adam: A method for stochastic optimization. In *International Conference on Learning Representations*, 2015. 13
- [16] Junnan Li, Dongxu Li, Silvio Savarese, and Steven Hoi. Blip-2: Bootstrapping language-image pre-training with frozen image encoders and large language models, 2023. 14
- [17] Kailin Li, Zhenxin Li, Shiyi Lan, Yuan Xie, Zhizhong Zhang, Jiayi Liu, Zuxuan Wu, Zhiding Yu, and Jose M Alvarez. Hydra-mdp++: Advancing end-to-end driving via expert-guided hydra-distillation. *arXiv preprint arXiv:2503.12820*, 2025. 2, 3, 6
- [18] Peidong Li and Dixiao Cui. Navigation-guided sparse scene representation for end-to-end autonomous driving. In *The Thirteenth International Conference on Learning Representations*, 2025. 3
- [19] Qifeng Li, Xiaosong Jia, Shaobo Wang, and Junchi Yan. Think2drive: Efficient reinforcement learning by thinking with latent world model for autonomous driving (in carla-v2). In *European Conference on Computer Vision*, pages 142–158. Springer, 2024. 6
- [20] Xiaofan Li, Yifu Zhang, and Xiaoqing Ye. Drivingdiffusion: layout-guided multi-view driving scenarios video generation with latent diffusion model. In *European Conference on Computer Vision*, pages 469–485. Springer, 2024. 3
- [21] Yingyan Li, Lue Fan, Jiawei He, Yuqi Wang, Yuntao Chen, Zhaoxiang Zhang, and Tieniu Tan. Enhancing end-to-end autonomous driving with latent world model. In *The Thirteenth International Conference on Learning Representations*, 2025. 3, 6, 7
- [22] Yingyan Li, Yuqi Wang, Yang Liu, Jiawei He, Lue Fan, and Zhaoxiang Zhang. End-to-end driving with online trajectory evaluation via bev world model. *arXiv preprint arXiv:2504.01941*, 2025. 2, 3, 6, 7, 8, 13, 14
- [23] Zhenxin Li, Kailin Li, Shihao Wang, Shiyi Lan, Zhiding Yu, Yishen Ji, Zhiqi Li, Ziyue Zhu, Jan Kautz, Zuxuan Wu, et al. Hydra-mdp: End-to-end multimodal planning with multi-target hydra-distillation. *arXiv preprint arXiv:2406.06978*, 2024. 2, 3, 6, 7
- [24] Zhiqi Li, Wenhai Wang, Hongyang Li, Enze Xie, Chonghao Sima, Tong Lu, Qiao Yu, and Jifeng Dai. Bevformer:

- learning bird’s-eye-view representation from lidar-camera via spatiotemporal transformers. *IEEE Transactions on Pattern Analysis and Machine Intelligence*, 2024. 4, 6, 13
- [25] Zhenxin Li, Wenhao Yao, Zi Wang, Xinglong Sun, Joshua Chen, Nadine Chang, Maying Shen, Zuxuan Wu, Shiyi Lan, and Jose M Alvarez. Generalized trajectory scoring for end-to-end multimodal planning. *arXiv preprint arXiv:2506.06664*, 2025. 2
- [26] Bencheng Liao, Shaoyu Chen, Haoran Yin, Bo Jiang, Cheng Wang, Sixu Yan, Xinbang Zhang, Xiangyu Li, Ying Zhang, Qian Zhang, et al. Diffusiondrive: Truncated diffusion model for end-to-end autonomous driving. In *Proceedings of the IEEE/CVF Conference on Computer Vision and Pattern Recognition*, pages 12037–12047, 2025. 6, 7, 8, 13, 14
- [27] Shuai Liu, Quanmin Liang, Zefeng Li, Boyang Li, and Kai Huang. Gaussianfusion: Gaussian-based multi-sensor fusion for end-to-end autonomous driving. In *The Thirty-ninth Annual Conference on Neural Information Processing Systems*, 2025. 6, 7
- [28] Chen Min, Dawei Zhao, Liang Xiao, Jian Zhao, Xinli Xu, Zheng Zhu, Lei Jin, Jianshu Li, Yulan Guo, Junliang Xing, et al. Driveworld: 4d pre-trained scene understanding via world models for autonomous driving. In *Proceedings of the IEEE/CVF Conference on Computer Vision and Pattern Recognition*, pages 15522–15533, 2024. 3
- [29] Aditya Prakash, Kashyap Chitta, and Andreas Geiger. Multimodal fusion transformer for end-to-end autonomous driving. In *Proceedings of the IEEE/CVF Conference on Computer Vision and Pattern Recognition*, pages 7077–7087, 2021. 6, 7, 13
- [30] Katrin Renz, Long Chen, Elahe Arani, and Oleg Sinavski. Simlingo: Vision-only closed-loop autonomous driving with language-action alignment. In *Proceedings of the IEEE/CVF Conference on Computer Vision and Pattern Recognition 2025*. IEEE, 2025. 14
- [31] ShuYao Shang, Yuntao Chen, Yuqi Wang, Yingyan Li, and Zhaoxiang Zhang. Drivedpo: Policy learning via safety dpo for end-to-end autonomous driving. In *The Thirty-ninth Annual Conference on Neural Information Processing Systems*, 2025. 7
- [32] Chonghao Sima, Katrin Renz, Kashyap Chitta, Li Chen, Hanxue Zhang, Chengen Xie, Jens Beißwenger, Ping Luo, Andreas Geiger, and Hongyang Li. Drivelm: Driving with graph visual question answering. In *Proceedings of the European Conference on Computer Vision 2024*, pages 256–274. Springer, 2024. 14
- [33] Ziyang Song, Caiyan Jia, Lin Liu, Hongyu Pan, Yongchang Zhang, Junming Wang, Xingyu Zhang, Shaoqing Xu, Lei Yang, and Yadan Luo. Don’t shake the wheel: Momentum-aware planning in end-to-end autonomous driving. In *Proceedings of the IEEE/CVF Conference on Computer Vision and Pattern Recognition*, pages 22432–22441, 2025. 2
- [34] Wenchao Sun, Xuewu Lin, Yining Shi, Chuang Zhang, Haoran Wu, and Sifa Zheng. Sparsedrive: End-to-end autonomous driving via sparse scene representation. In *2025 IEEE International Conference on Robotics and Automation (ICRA)*, pages 8795–8801. IEEE, 2025. 2, 3
- [35] Lening Wang, Wenzhao Zheng, Yilong Ren, Han Jiang, Zhiyong Cui, Haiyang Yu, and Jiwen Lu. Occsora: 4d occupancy generation models as world simulators for autonomous driving. *arXiv preprint arXiv:2405.20337*, 2024. 2
- [36] Xiaofeng Wang, Zheng Zhu, Guan Huang, Xinze Chen, Jiagang Zhu, and Jiwen Lu. Drivedreamer: Towards real-world-driven world models for autonomous driving. In *European Conference on Computer Vision*, pages 55–72. Springer, 2024. 3
- [37] Yuqi Wang, Jiawei He, Lue Fan, Hongxin Li, Yuntao Chen, and Zhaoxiang Zhang. Driving into the future: Multiview visual forecasting and planning with world model for autonomous driving. In *Proceedings of the IEEE/CVF Conference on Computer Vision and Pattern Recognition*, pages 14749–14759, 2024. 3
- [38] Xinshuo Weng, Boris Ivanovic, Yan Wang, Yue Wang, and Marco Pavone. Para-drive: Parallelized architecture for real-time autonomous driving. In *Proceedings of the IEEE/CVF Conference on Computer Vision and Pattern Recognition*, pages 15449–15458, 2024. 2, 3, 6, 7
- [39] Sanghyun Woo, Shoubhik Debnath, Ronghang Hu, Xinlei Chen, Zhuang Liu, In So Kweon, and Saining Xie. Convnext v2: Co-designing and scaling convnets with masked autoencoders. In *Proceedings of the IEEE/CVF Conference on Computer Vision and Pattern Recognition*, pages 16133–16142, 2023. 5
- [40] Penghao Wu, Xiaosong Jia, Li Chen, Junchi Yan, Hongyang Li, and Yu Qiao. Trajectory-guided control prediction for end-to-end autonomous driving: A simple yet strong baseline. *Advances in Neural Information Processing Systems*, 35:6119–6132, 2022. 7
- [41] Zebin Xing, Xingyu Zhang, Yang Hu, Bo Jiang, Tong He, Qian Zhang, Xiaoxiao Long, and Wei Yin. Goalflow: Goal-driven flow matching for multimodal trajectories generation in end-to-end autonomous driving. In *Proceedings of the IEEE/CVF Conference on Computer Vision and Pattern Recognition*, pages 1602–1611, 2025. 6, 7
- [42] Yan Yan, Yuxing Mao, and Bo Li. Second: Sparsely embedded convolutional detection. *Sensors*, 18(10):3337, 2018. 4, 6
- [43] Yu Yang, Jianbiao Mei, Yukai Ma, Siliang Du, Wenqing Chen, Yijie Qian, Yuxiang Feng, and Yong Liu. Driving in the occupancy world: Vision-centric 4d occupancy forecasting and planning via world models for autonomous driving. In *Proceedings of the AAAI Conference on Artificial Intelligence*, pages 9327–9335, 2025. 2
- [44] Wenhao Yao, Zhenxin Li, Shiyi Lan, Zi Wang, Xinglong Sun, Jose M Alvarez, and Zuxuan Wu. Drivesuprim: Towards precise trajectory selection for end-to-end planning. *arXiv preprint arXiv:2506.06659*, 2025. 2, 3, 6
- [45] Rui Yu, Xianghang Zhang, Runkai Zhao, Huaicheng Yan, and Meng Wang. Distilldrive: End-to-end multi-mode autonomous driving distillation by isomorphic hetero-source planning model. In *Proceedings of the IEEE/CVF International Conference on Computer Vision*, pages 26188–26197, 2025. 6, 7

- [46] Bozhou Zhang, Nan Song, Xin Jin, and Li Zhang. Bridging past and future: End-to-end autonomous driving with historical prediction and planning. In *Proceedings of the IEEE/CVF Conference on Computer Vision and Pattern Recognition*, pages 6854–6863, 2025. [2](#), [7](#)
- [47] Bozhou Zhang, Nan Song, Xiatian Zhu, Jiankang Deng, Li Zhang, et al. Future-aware end-to-end driving: Bidirectional modeling of trajectory planning and scene evolution. In *The Thirty-ninth Annual Conference on Neural Information Processing Systems*, 2025. [2](#), [3](#), [6](#)
- [48] Kaiwen Zhang, Zhenyu Tang, Xiaotao Hu, Xingang Pan, Xiaoyang Guo, Yuan Liu, Jingwei Huang, Li Yuan, Qian Zhang, Xiao-Xiao Long, Xun Cao, and Wei Yin. Epona: Autoregressive diffusion world model for autonomous driving. In *Proceedings of the IEEE/CVF International Conference on Computer Vision (ICCV)*, 2025.
- [49] Wenzhao Zheng, Weiliang Chen, Yuanhui Huang, Borui Zhang, Yueqi Duan, and Jiwen Lu. Occworld: Learning a 3d occupancy world model for autonomous driving. In *European Conference on Computer Vision*, pages 55–72. Springer, 2024. [2](#), [3](#)
- [50] Xizhou Zhu, Weijie Su, Lewei Lu, Bin Li, Xiaogang Wang, and Jifeng Dai. Deformable detr: Deformable transformers for end-to-end object detection. In *ICLR*, 2021. [4](#)

Supplementary Materials for SafeDrive

In these Supplementary Materials, we provide additional details that could not be included in the main paper due to space limitations. They include the following:

- Detailed Evaluation Metrics
- Additional Implementation Details
- Extensive Experimental Analysis
- Comprehensive Qualitative Results

A. Detailed Evaluation Metrics

A.1. NAVSIM Dataset

PDM Score (PDMS). PDMS evaluates driving performance using safety, progress, and comfort metrics computed in a non-reactive simulation of the predicted trajectory. Safety-critical violations such as collisions and lane departures yield a zero score through multiplicative penalties, and all remaining subscores are aggregated by a weighted average. The metrics and their weights are summarized in Table 7, and PDMS is defined as

$$\text{PDMS} = \left(\prod_{m \in \mathcal{P}} s_m \right) \left(\frac{\sum_{m \in \mathcal{W}} w_m s_m}{\sum_{m \in \mathcal{W}} w_m} \right), \quad (8)$$

where $\mathcal{P} = \{\text{NC}, \text{DAC}\}$ and $\mathcal{W} = \{\text{EP}, \text{TTC}, \text{C}\}$ denote the penalty and weighted metric sets, respectively, and s_m and w_m denote the score and weight of each metric. PDMS is computed per frame and averaged over the full sequence.

Extended PDM Score (EPDMS). PDMS assigns penalties even when the human driver also violates a rule and does not consider rule-based behaviors such as traffic-light compliance. EPDMS addresses these limitations by filtering out human-caused violations and introducing additional evaluation metrics. Newly added metrics are listed in Table 7, and all others except Comfort are inherited from PDMS. EPDMS is defined as

$$\tilde{s}_m = \begin{cases} 1 & s_m^{\text{human}} = 0 \\ s_m^{\text{pred}} & \text{otherwise} \end{cases} \quad (9)$$

$$\text{EPDMS} = \left(\prod_{m \in \mathcal{P}_{\text{ext}}} \tilde{s}_m \right) \left(\frac{\sum_{m \in \mathcal{W}_{\text{ext}}} w_m \tilde{s}_m}{\sum_{m \in \mathcal{W}_{\text{ext}}} w_m} \right), \quad (10)$$

where s_m^{pred} and s_m^{human} denote the values computed from the predicted and human trajectories, respectively. The sets $\mathcal{P}_{\text{ext}} = \{\text{NC}, \text{DAC}, \text{DDC}, \text{TLC}\}$ and $\mathcal{W}_{\text{ext}} = \{\text{EP}, \text{TTC}, \text{LK}, \text{HC}, \text{EC}\}$ represent the penalty and weighted metrics.

Table 7. Metrics used in PDMS and EPDMS. "*" indicates metrics used only in PDMS.

| Metric | EPDMS only | Weight | Range |
|--------------------------------------|------------|------------|-------------|
| No at-fault Collisions (NC) | | multiplier | {0, 1/2, 1} |
| Drivable Area Compliance (DAC) | | multiplier | {0, 1} |
| Driving Direction Compliance (DDC) | ✓ | multiplier | {0, 1/2, 1} |
| Traffic Light Compliance (TLC) | ✓ | multiplier | {0, 1} |
| Ego Progress (EP) | | 5 | [0, 1] |
| Time to Collision (TTC) within bound | | 5 | {0, 1} |
| Comfort (C)* | | 2 | {0, 1} |
| Lane Keeping (LK) | ✓ | 2 | {0, 1} |
| History Comfort (HC) | ✓ | 2 | {0, 1} |
| Extended Comfort (EC) | ✓ | 2 | {0, 1} |

A.2. Bench2Drive Benchmark

Driving Score (DS). DS evaluates the overall driving performance by combining route completion with penalties for safety-related infractions. For each route, the score is obtained by multiplying the route-completion percentage by the infraction penalties defined in Table 8. DS is computed as

$$\text{DS} = \frac{1}{n_{\text{total}}} \sum_{i=1}^{n_{\text{total}}} \text{RC}^i \cdot \prod_{j=1}^{n_{\text{penalty}}^i} p_j^i, \quad (11)$$

where n_{total} is the number of routes, RC^i is the route-completion percentage for route i , p_j^i is the penalty factor for the j -th infraction on route i , and n_{penalty}^i is the number of infractions considered for that route.

Table 8. Infraction types and penalty factors used in the DS.

| Infraction | Penalty | Note |
|----------------------|---------|-------------------|
| Pedestrian Collision | 0.50 | Each occurrence |
| Vehicle Collision | 0.60 | Each occurrence |
| Other Collision | 0.65 | Each occurrence |
| Running Red Light | 0.70 | Each occurrence |
| Scenario Timeout | 0.70 | Timeout (4 min) |
| Too Slow | 0.70 | Low speed |
| No Give Way | 0.70 | Yield failure |
| Off-road | - | Excluded from RC |
| Route Deviation | - | Deviation > 30 m |
| Agent Blocked | - | Idle for 180 s |
| Route Timeout | - | Max time exceeded |

Success Rate (SR). SR measures the proportion of routes that are successfully completed among all evaluation routes. A route is considered successful only if the ego vehicle reaches the goal destination within the time limit without committing any infractions. SR is computed as the ratio between the number of successful routes n_{success} and the total number of evaluation routes n_{total} , as follows:

$$\text{SR} = \frac{n_{\text{success}}}{n_{\text{total}}}. \quad (12)$$

B. Additional Implementation Details

We used four H100 80GB GPUs, with a batch size of 32 per GPU for perception pretraining and 16 for full-model training. End-to-end training was conducted for 60 + 15 epochs on NAVSIM [5] and 20 + 15 epochs on Bench2Drive [11], using the Adam [15] optimizer with a cosine learning rate schedule and warmup.

Existing studies [22, 26, 29] typically apply a BEV segmentation auxiliary task after the BEV backbone. In our model, we also employ BEV segmentation as an auxiliary task after the BEV backbone, in addition to object detection for SWNet and static BEV segmentation for TwDAC. Prior works generally operate with a perception range of [0, 32] m forward and [-32, 32] m laterally and adopt a 0.25 m resolution for BEV segmentation. To enhance safety by incorporating long-range contextual cues, we extend the forward perception range to [0, 64] m and increase the BEV resolution to 0.125 m, thereby providing richer spatial information. We further stabilize motion prediction by incorporating image and LiDAR inputs from the current frame and two past frames. We also redesign the object detection decoder following the iterative refinement mechanism of [24].

C. Extensive Experimental Analysis

Effect of Perception Performance to Planning. Table 9 presents the ablation results comparing different BEV backbones and planning heads. TransFuser [29] differs only in its feature encoding, while sharing the same perception range, object decoder, and related settings as BEVFormer [24]. SafeDrive is slower than DiffusionDrive [26] due to its fine-grained safety reasoning process, yet it consistently achieves higher planning performance across all configurations. Notably, DiffusionDrive shows limited planning improvements even when its perception performance increases, whereas SafeDrive yields a substantial PDMS gain when combined with the BEVFormer backbone. This indicates that perceptual outputs in DiffusionDrive do not directly influence the generated trajectories, while SafeDrive effectively leverages high-fidelity perceptual representations within its safety-critical reasoning process to produce safer trajectories.

Impact of Trajectory Refinement. Table 10 presents the ablation study on trajectory refinement. When the initial anchor trajectories are used without any refinement, the PDMS remains at 88.1. Refining ProposalNet alone raises the score to 90.6, and adding planning-branch refinement in SWNet further improves it to 90.9. Incorporating surrounding-agent motion refinement achieves the highest PDMS of 91.6. These results show that refining the motions of surrounding agents in SWNet more accurately

Table 9. Ablation study on BEV backbone and planning head. "TF", "BF", and "Diff" denote TransFuser, BEVFormer, and DiffusionDrive, respectively.

| Backbone | Head | mAP | mIoU | NC | DAC | PDMS | Latency (ms) |
|----------|------|-------------|-------------|-------------|-------------|-------------|--------------|
| TF | Diff | 53.2 | 45.6 | 98.4 | 96.2 | 88.3 | 40 |
| TF | Ours | 51.8 | 44.7 | 99.0 | 97.3 | 89.6 | 55 |
| BF | Diff | 91.4 | 56.4 | 98.8 | 96.3 | 88.6 | 50 |
| BF | Ours | 86.6 | 54.7 | 99.5 | 99.0 | 91.6 | 67 |

Table 10. Ablation study on the impact of trajectory refinement

| ProposalNet Refinement | SWNet Refinement Planning | SWNet Refinement Motion | NC | DAC | TTC | PDMS |
|------------------------|---------------------------|-------------------------|-------------|-------------|-------------|-------------|
| | | | 98.4 | 96.9 | 93.6 | 88.1 |
| ✓ | | | 99.1 | 98.0 | 96.5 | 90.6 |
| ✓ | ✓ | | 99.1 | 98.3 | 96.7 | 90.9 |
| ✓ | ✓ | ✓ | 99.5 | 99.0 | 97.2 | 91.6 |

Table 11. Comparison of collision-avoidance methods. Conflict Filtering removes trajectories overlapping with predicted agent motions.

| Method | NC | DAC | TTC | PDMS |
|--------------------|-------------|-------------|-------------|-------------|
| Scene-Level NC | 99.2 | 98.2 | 96.7 | 90.9 |
| Conflict Filtering | 99.3 | 98.2 | 96.8 | 91.0 |
| Pair-wise NC | 99.5 | 98.7 | 97.3 | 91.5 |

Table 12. Ablation of TwDAC Components. Temporal predicts and evaluates drivable-area compliance at each time step. Interpolated enhances compliance checking using bilinear interpolation over the predicted BEV segmentation.

| Temporal | Interpolated | NC | DAC | TTC | PDMS |
|----------|--------------|-------------|-------------|-------------|-------------|
| | | 99.2 | 98.2 | 96.7 | 90.9 |
| ✓ | | 99.2 | 98.7 | 96.7 | 91.2 |
| | ✓ | 99.2 | 98.5 | 96.6 | 91.1 |
| ✓ | ✓ | 99.2 | 99.0 | 96.7 | 91.4 |

captures instance-centric interactions between the planning query and nearby agents, which directly contributes to generating more stable and safer trajectories.

Comparison of Collision-Avoidance Methods. As shown in Table 11, we compare three methods for evaluating collision-avoidance capability. Conflict Filtering, which removes trajectories overlapping with predicted agent motions, produces results similar to Scene-Level NC (NC 99.3). Pair-wise NC enhances safety-critical decision making by explicitly modeling interactions between the planning trajectory and nearby agents, improving NC to 99.5 and TTC to 97.3. These gains are notable given the already high baseline and arise from more fine-grained assessment of collision risks.

Ablation Study for TwDAC Table 12 reports the effect of the two TwDAC components. Without either component, the model attains a DAC of 98.2. Adding the Temporal evaluation improves it to 98.7, and using only the interpolation-based evaluation yields a comparable increase to 98.5. Combining both achieves the highest DAC of 99.0. These results indicate that each component enhances drivable-area compliance estimation, and that combining them enables a more fine-grained assessment of drivable-area safety.

D. Comprehensive Qualitative Results

More Visualizations of Fine-grained Reasoning. Figure 5 visualizes the fine-grained safety reasoning process of SafeDrive. For each scenario, the bottom-left panel illustrates the fine-grained safety scores—(a) PwNC and (b) TwDAC—predicted from the simulated future states of each candidate trajectory. The bottom-right panel of each scenario then shows the final trajectory selection guided by these safety signals. In contrast to ProposalNet, which often selects unsafe trajectories due to its scene-level safety estimates, FRNet leverages the fine-grained safety information from PwNC and TwDAC to choose safer trajectories. These precise and interpretable safety cues obtained through the simulation process provide essential guidance for reliable and safe trajectory selection.

Additional Comparison with SOTA Methods. Figures 6 and 7 qualitatively compare SOTA models [22, 26] across diverse scenarios. SafeDrive, in particular, produces safety-oriented trajectories by modeling fine-grained interactions with surrounding agents and the environment.

Visualization of the Bench2Drive Benchmark. Figure 8 illustrates that SafeDrive also achieves robust closed-loop driving performance across diverse and challenging scenarios in the Bench2Drive benchmark.

Failure Case. Figure 9 presents a failure where SafeDrive collides with a pedestrian stepping out of a vehicle. Although the model generates a forward trajectory at time t that does not hit the stopped vehicle, it fails to reason about the pedestrian emerging from the slightly opening door. This reveals that the model struggles to interpret subtle contextual cues associated with human behavior. Addressing such cases may require integrating VLM-based [2, 16, 30, 32] semantic reasoning with our framework to better capture these contextual signals and produce safer motion plans.

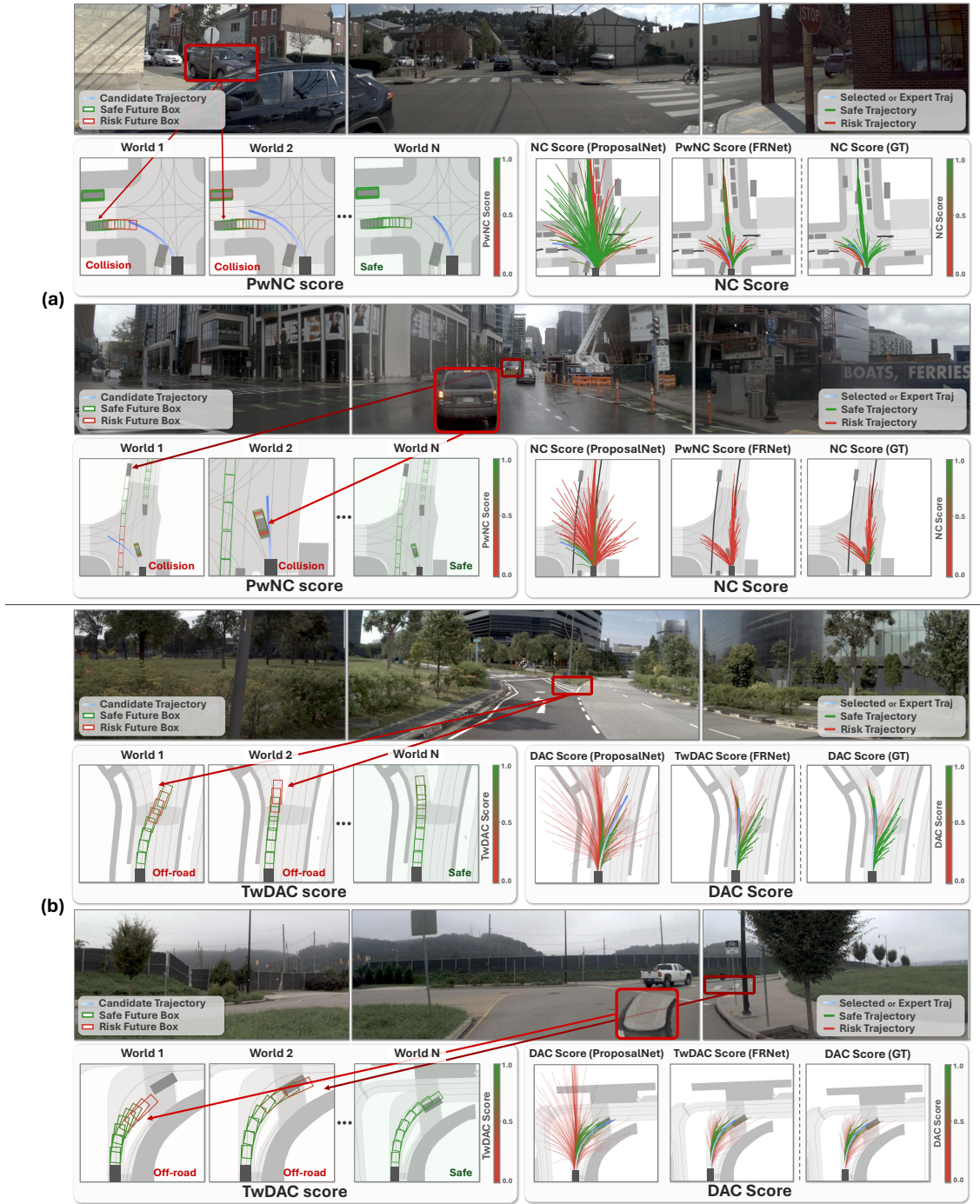


Figure 5. **Visualization of reasoning process.** The figure compares two forms of fine-grained safety reasoning, PwNC in (a) and TwDAC in (b). The bottom-left panel visualizes predicted fine-grained safety scores across Sparse Worlds using red-green shading, with (a) visualizing PwNC scores for the future boxes of surrounding agents and (b) visualizing TwDAC scores for the future ego boxes. The bottom-right panel presents the corresponding trajectory-level scores, showing NC scores for (a) and DAC scores for (b), each generated by ProposalNet, FRNet, and the ground truth.

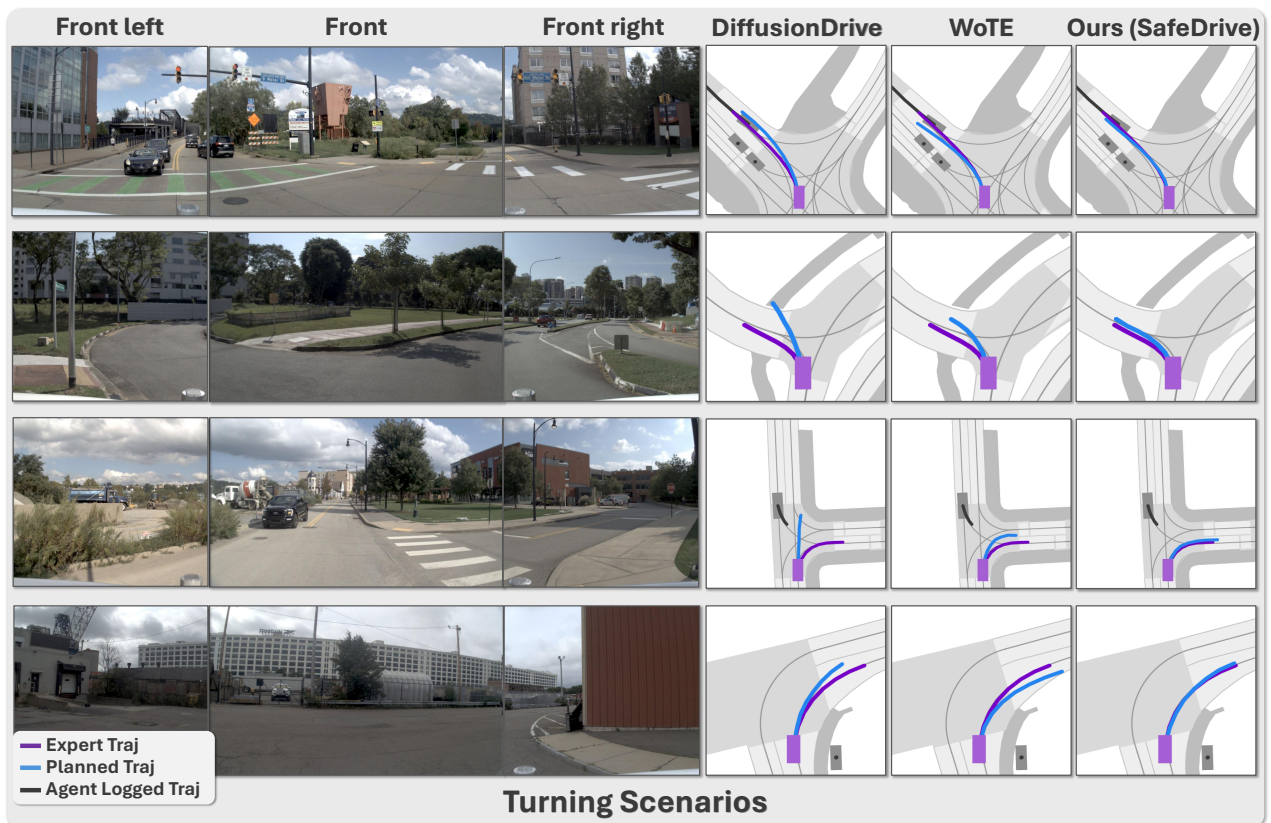
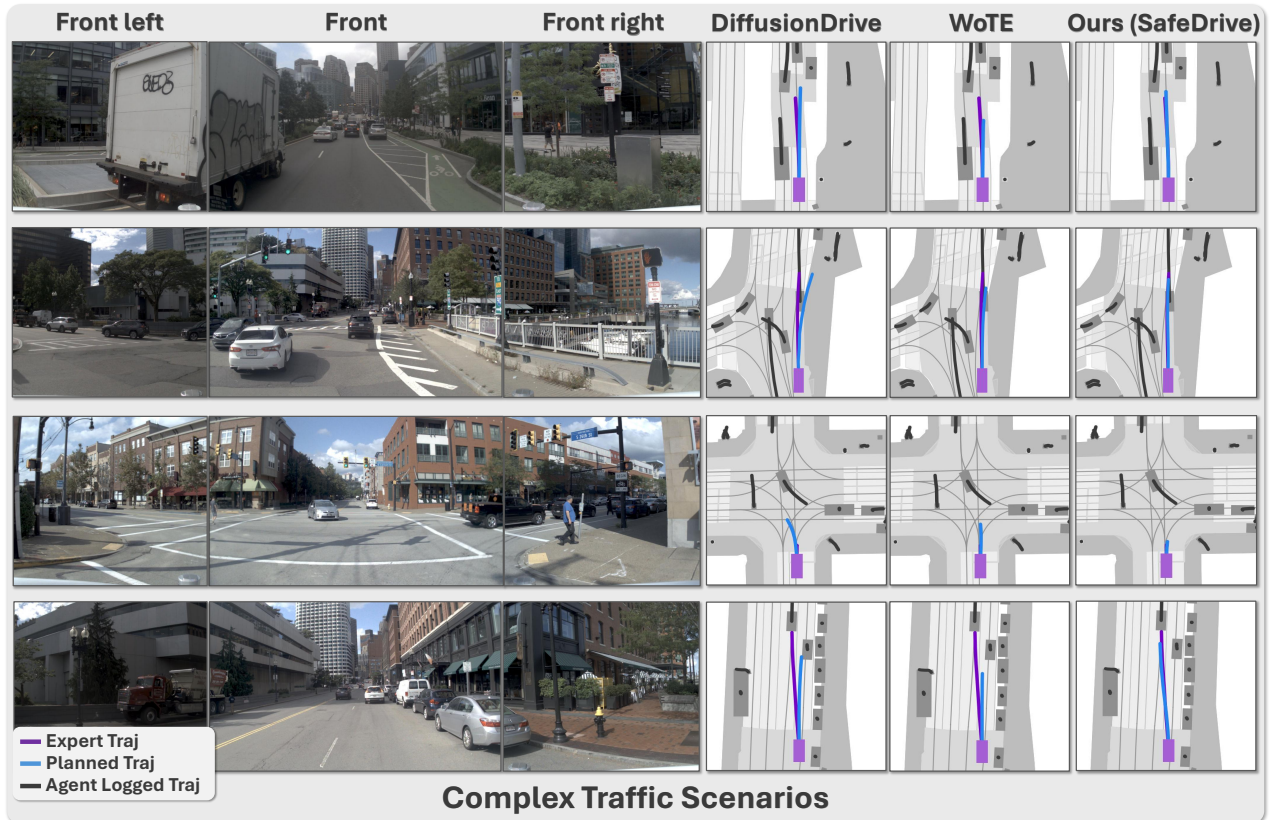


Figure 6. **Additional Comparison with SOTA methods.** Qualitative comparisons of DiffusionDrive, WoTE, and SafeDrive in complex traffic scenarios and turning scenarios.

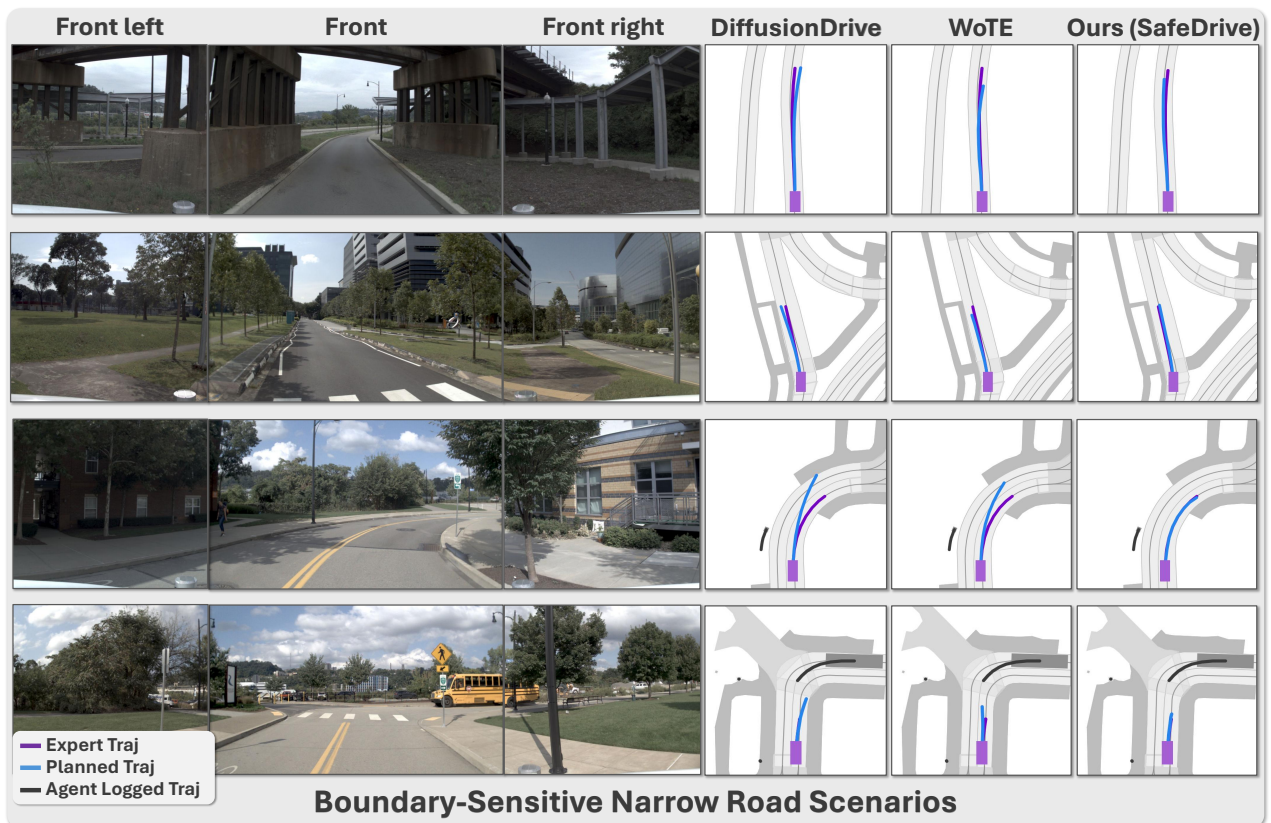
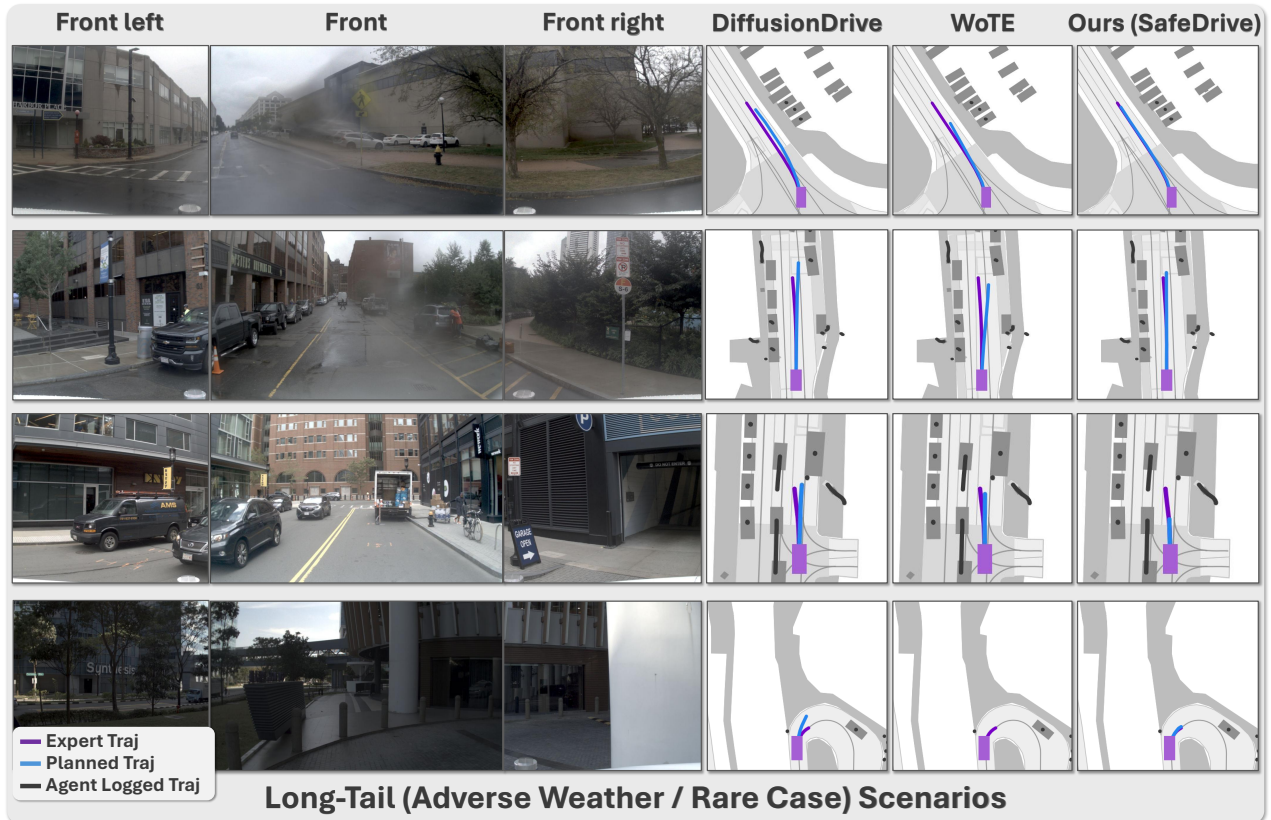


Figure 7. **Additional Comparison with SOTA methods.** Qualitative comparisons of DiffusionDrive, WoTE, and SafeDrive in long-tail scenarios and boundary-sensitive narrow road scenarios.

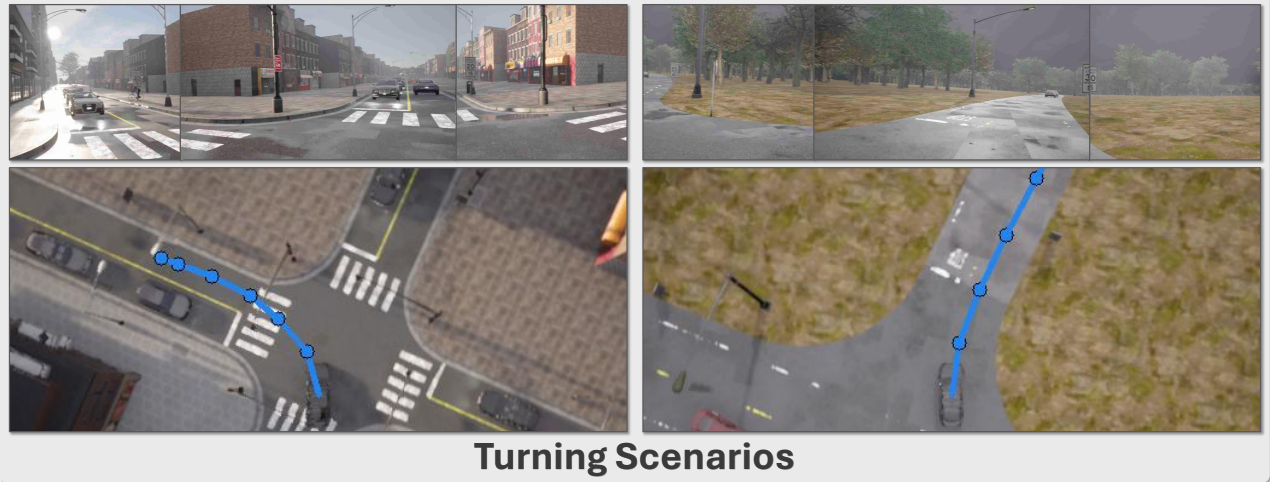


Figure 8. **Visualization of the Bench2Drive benchmark.** The predicted trajectories are visualized as blue curves in each scene. SafeDrive demonstrates robust performance across diverse scenarios in closed-loop environments, consistently generating stable and safe motions.



Figure 9. **Failure Case: Inability to Anticipate Pedestrian Exit from an Opening Door.** At time t , SafeDrive generates a trajectory that continues in its lane without colliding with the stopped vehicle, but the predicted ego path eventually collides with a pedestrian who steps out of the vehicle as the door is opening. This occurs because SafeDrive fails to incorporate the contextual cue that a slightly open door may indicate an imminent pedestrian exit. This case highlights the need for a more comprehensive understanding of contextual cues in the scene, beyond simply recognizing the current and past positions of vehicles and pedestrians.